

# Simulations of ultracold bosonic atoms in optical lattices with anharmonic traps

Olivier Gygi, Helmut G. Katzgraber, and Matthias Troyer  
*Theoretische Physik, ETH Zürich, CH-8093 Zürich, Switzerland*

Stefan Wessel  
*Institut für Theoretische Physik III, Universität Stuttgart, 70550 Stuttgart, Germany*

G. George Batrouni  
*Institut Non-Linéaire de Nice, UMR CNRS 6618, Université de Nice-Sophia Antipolis, 1361 route des Lucioles, F-06560 Valbonne, France*  
(Dated: December 2, 2024)

We report results of quantum Monte Carlo simulations in the canonical and the grand-canonical ensemble of the two- and three-dimensional Bose-Hubbard model with quadratic and quartic confining potentials. The quantum criticality of the superfluid–Mott insulator transition is investigated both on the boundary layer separating the two coexisting phases and at the center of the traps where the Mott-insulating phase is first established. Recent simulations of systems in quadratic traps have shown that the transition is not in the critical regime due to the finite gradient of the confining potential and that critical fluctuations are suppressed. In addition, it has been shown that quantum critical behavior is recovered in flat confining potentials as they approach the uniform regime. Our results show that quartic traps display a behavior similar to quadratic ones, yet locally at the center of the traps the bulk transition has enhanced critical fluctuations in comparison to the quadratic case. Therefore quartic traps provide a better prerequisite for the experimental observation of true quantum criticality of ultracold bosonic atoms in optical lattices.

PACS numbers: 73.43.Nq, 05.30.Jp, 03.75.Lm

## I. INTRODUCTION

The Bose-Hubbard model offers an almost perfect description of Bose-Einstein condensates in optical lattices [1, 2]. Therefore the model has been intensively studied both analytically [1, 3, 4, 5] as well as numerically [6, 7, 8, 9, 10, 11, 12, 13] in recent years. In the absence of a trapping potential, i.e., for the *homogeneous Bose-Hubbard model*, a quantum phase transition from a superfluid to a Mott-insulating phase occurs at commensurate fillings upon increasing the optical lattice depth [3]. Experimentally, Bose-Einstein condensates are created by cooling bosonic atoms. In order to prevent them from evaporating, they must be trapped by a confining potential. As shown for example in Ref. 11, inhomogeneous confining potentials induce a coexistence of superfluid and Mott-insulating regions for a continuous range of incommensurate fillings. By a suitable increase of the lattice depth and the number of particles, one may start forming a Mott-insulating region in the center of the trap. A further increase of the lattice depth induces a change of the volume fractions between the two phases. Accordingly, the transition recently observed in experiments of ultracold Bose gases in optical lattices embedded in quadratic confining potentials [2] should be better viewed as a crossover with changing volume fractions of the two phases [12] rather than as a true phase transition.

Although globally no true transition can be observed in systems with inhomogeneous traps, one might expect to observe a superfluid–Mott insulator transition on the boundary layer separating the coexisting superfluid and

Mott-insulating regions and, locally, at the center of the trap where the Mott-insulating phase has been established. In the following we distinguish these transitions by referring to them as “surface transition” and “bulk transition,” respectively. Recent quantum Monte Carlo simulations of the Bose-Hubbard model in quadratic confining potentials have shown that the quantum criticality of these transitions is destroyed by the finite gradient of the confining potential [12]. However it has been demonstrated that quantum criticality is recovered in flat traps where the potential gradient becomes irrelevant in the center, i.e., when locally the trap center approaches the uniform regime.

Here we study flat anharmonic traps, which can be experimentally realized, e.g., by superimposing pairs of weak, repulsive, blue-detuned Gaussian laser beams to pairs of attractive, red-detuned Gaussian laser beams that create the optical lattice. Depending on the beam parameters, it is possible to cancel out the harmonic terms in the series expansion of the resulting potential. In our simulations with anharmonic traps we consider only fourth-order terms in the expansion and neglect all higher-order ones. The results we have obtained from our simulations of two-dimensional (2D) systems in quartic traps and the comparison to our results for systems in quadratic traps, closed-box systems confined by completely flat and infinitely sharp traps, as well as homogeneous systems with periodic boundary conditions clearly demonstrate that the surface transition in systems with quartic traps has the same lack of quantum criticality as the corresponding transition in the sys-

tems with quadratic traps. However, the bulk transition has stronger critical fluctuations in the center of quartic traps, than in the center of quadratic traps. These observations lead us to the conclusion that quantum criticality in systems with inhomogeneous traps is determined by the flatness in the trap centers and their closest surroundings, i.e., by the smaller deviation from the uniform regime, and not by the shape and steepness of the walls. Thus, quartic traps could provide a better prerequisite for future experimental observations of true quantum criticality.

We also present results on three-dimensional (3D) systems with smaller system sizes which qualitatively show the same results as in two space dimensions, albeit less pronounced.

The paper is organized as follows: In Sec. II we introduce in detail both the Bose-Hubbard model with the specific traps that we have used and the observables needed for the investigations of the systems. In Sec. III we present our results, and in Sec. IV we summarize our observations.

## II. MODEL, OBSERVABLES, AND NUMERICAL DETAILS

In order to describe trapped ultracold bosonic atoms in optical lattices we use the Bose-Hubbard Hamiltonian

$$\mathcal{H} = -t \sum_{\langle i,j \rangle} (\hat{b}_i^\dagger \hat{b}_j + \text{H.c.}) + \frac{U}{2} \sum_i \hat{n}_i (\hat{n}_i - 1) - \mu_0 \sum_i \hat{n}_i + \sum_i V(i) \hat{n}_i, \quad (1)$$

where  $\hat{b}_i^\dagger$  and  $\hat{b}_i$  are the creation and annihilation operators for bosons at lattice sites  $i$ , respectively, and

$$\hat{n}_i = \hat{b}_i^\dagger \hat{b}_i \quad (2)$$

is the local density operator.  $t$  represents the nearest-neighbor hopping matrix element,  $U$  the onsite repulsion,  $\mu_0$  a chemical potential offset that controls the filling of the trap and  $V(i)$  the trap potential. The two last terms of the Hamiltonian can be conveniently combined by defining an effective, spatially-dependent chemical potential  $\mu_i^{\text{eff}}$  that is experienced by a boson at site  $i$ , i.e.,

$$\mu_i^{\text{eff}} = \mu_0 - V(i). \quad (3)$$

Due to the inhomogeneity introduced by a trapping potential needed for the confinement of the atoms in experimental realizations of the Bose-Hubbard model, it becomes necessary to consider local, site-dependent quantities, in contrast to the homogeneous Bose-Hubbard model, where it suffices to measure global quantities such as the global compressibility and the superfluid density [14] to capture the system characteristics. One way of distinguishing coexisting local superfluid and Mott-insulating states in systems with traps is to investigate

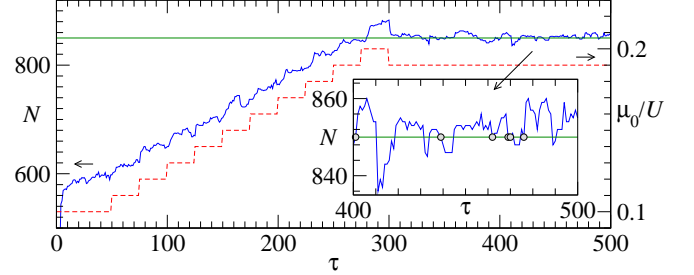


FIG. 1: (Color online) Evolution of the measured particle number  $N$  (solid curve) toward the desired value  $N = 850$  while adjusting the chemical potential offset  $\mu_0/U$  (dashed curve) at the beginning of the thermalization phase. The system size is  $50 \times 50$  in a quartic trap. The inset is a detailed view of  $N$  fluctuating around  $N = 850$  as a function of time. The circles indicate the configurations for which  $N$  is exactly 850 and which can be used in a canonical measurement.

the topology of local density profiles. Regions with constant integer fillings can be interpreted to be Mott-insulating, whereas regions with noninteger fillings must be superfluid. The local compressibility  $\kappa_i^{\text{local}}$  at site  $i$ ,

$$\kappa_i^{\text{local}} = \frac{\partial \langle N \rangle}{\partial \mu_i^{\text{eff}}} = \int_0^\beta d\tau [\langle \hat{n}_i(\tau) N \rangle - \langle \hat{n}_i(\tau) \rangle \langle N \rangle], \quad (4)$$

provides a more precise way to distinguish the local states and to probe for quantum criticality. It expresses the response of the system's particle number  $N$  to a local change of the effective chemical potential  $\mu_i^{\text{eff}}$  at site  $i$ . In the above equation,  $\beta = 1/k_B T$  denotes the inverse temperature,

$$\hat{n}_i(\tau) = \exp(\tau \mathcal{H}) n_i \exp(-\tau \mathcal{H}) \quad (5)$$

the imaginary-time propagated operator, and  $\langle \dots \rangle$  the Monte Carlo sample average. Note that this definition of the local compressibility only makes sense in the grand-canonical ensemble where the total number of particles  $N$  in the system is variable, since otherwise the integrand vanishes and the local compressibility is zero everywhere.

The measurement of local density fluctuations provides another way of investigating the local states of inhomogeneous systems. In addition to measuring the variance of the local density,

$$\Delta_i = \langle n_i^2 \rangle - \langle n_i \rangle^2, \quad (6)$$

it can be useful to measure the onsite compressibility  $\kappa_i^{\text{onsite}}$ , i.e., the response of the local density at site  $i$  to a chemical potential change at this site,

$$\kappa_i^{\text{onsite}} = \frac{\partial \langle n_i \rangle}{\partial \mu_i^{\text{eff}}} = \int_0^\beta d\tau [\langle \hat{n}_i(\tau) \hat{n}_i(0) \rangle - \langle \hat{n}_i(\tau) \rangle \langle \hat{n}_i(0) \rangle]. \quad (7)$$

For our simulations, we have used two worm-like quantum Monte Carlo algorithms provided by the ALPS project [15], the worm algorithm [16] and the stochastic

TABLE I: Overview of the simulations with quadratic and quartic traps in 2D simulated in the canonical ensemble.  $N$  is the fixed particle number at which the observables are evaluated in the canonical ensemble,  $\mu_0/U$  and  $t/U$  are the chemical potential offset and the hopping parameter in units of the interaction parameter  $U$ , respectively.  $a_2$  and  $a_4$  are the curvatures of the quadratic and quartic traps.

size	trap curvature	$N$	$\mu_0/U$	$t/U$
$50^2$	$a_4/U = 3.5 \cdot 10^{-6}$	1200	0.362	0.04
$50^2$	$a_2/U = 2 \cdot 10^{-3}$	600	0.370	0.04

series expansion (SSE) algorithm with directed loops [17]. Both algorithms work generically in the grand-canonical ensemble. Since experiments are usually performed with a fixed number of particles, we want our simulations to also be performed with a fixed particle number, i.e., in the canonical ensemble. For this purpose, we have applied some modifications to the algorithms to fit our needs. In order for the Hamiltonian in Eq. (1) to be fully defined, the correct chemical potential offset  $\mu_0/U$ , which yields the desired particle number  $N$  at which the simulations are to be performed, has to be determined. Starting from a guess value the correct value of  $\mu_0/U$  is approximated at the beginning of the thermalization phase of the simulation, as illustrated in Fig. 1. The dashed curve shows the subsequent adjustments of the chemical potential offset  $\mu_0/U$  and the solid curve represents the evolution of the measured particle number, which equilibrates around the desired particle number  $N$  (solid, horizontal line) once the adjustment of  $\mu_0/U$  is complete.

Measuring observables in the canonical ensemble is then simply done by measuring the particle number after each Monte Carlo step and by selecting out only updated configurations for which the measured particle number coincides with the desired particle number at which the simulations are meant to be performed. By computing the Monte Carlo sample averages using only the selected updated configurations, the observables are evaluated in the canonical ensemble, whereas by including all other updated configurations for the computation of the sample averages, the observables are evaluated in the grand-canonical ensemble.

We have found no substantial qualitative deviations between the canonical and grand-canonical data for all observables. In Figs. 3 and 4 we plot the data evaluated in the canonical ensemble, except for the local compressibility, which, for reasons mentioned above, cannot be measured canonically. In Figs. 5, 7 and 8, where comparisons are made with uniform systems, we have chosen to plot the data evaluated in the grand-canonical ensemble, since obtaining the different curves for the uniform systems implies that the filling is allowed to change [18].

The 2D and 3D trapping potentials we have used are

$$V_{2D}^{(2)} = a_2 (x^2 + y^2) \quad (8)$$

$$V_{2D}^{(4)} = a_4 (x^4 + y^4) \quad (9)$$

TABLE II: Overview of the simulations with quadratic and quartic traps in 2D (top) and 3D (bottom) simulated in the grand-canonical ensemble.  $N$  is the particle number and  $\mu_{\text{center}}^{\text{eff}}/U$  and  $t/U$  are the effective chemical potential at the central lattice sites [19] and the hopping parameter in units of the interaction parameter  $U$ , respectively.  $a_2$  and  $a_4$  are the curvatures of the quadratic and quartic traps.

size	trap curvature	$N$	$\mu_{\text{center}}^{\text{eff}}/U$	$t/U$
$50^2$	$a_4/U = 3.5 \cdot 10^{-6}$	908 – 924	0.217	0.01 – 0.06
$50^2$	$a_2/U = 2 \cdot 10^{-3}$	341 – 413	0.217	0.01 – 0.06
$14^3$	$a_4/U = 7 \cdot 10^{-4}$	462 – 498	0.217	0.006 – 0.04
$14^3$	$a_2/U = 3 \cdot 10^{-2}$	90 – 122	0.217	0.006 – 0.04

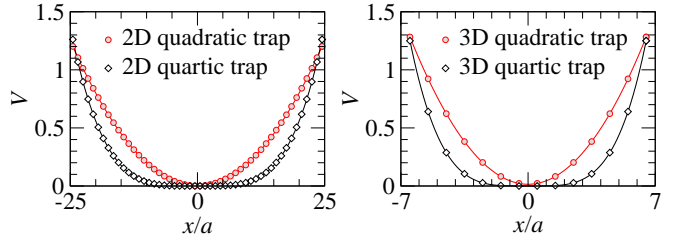


FIG. 2: (Color online) Sections  $V(x, y = a/2)$  and  $V(x, y = a/2, z = a/2)$  through the 2D (left) and 3D (right) traps that have been used in the simulations. The simulation parameters are summarized in Tables I and II. The points indicate the lattice sites separated by the lattice constant  $a$ .

$$V_{3D}^{(2)} = a_2 (x^2 + y^2 + z^2) \quad (10)$$

$$V_{3D}^{(4)} = a_4 (x^4 + y^4 + z^4), \quad (11)$$

where the trap curvatures are given in Tables I and II (see also Fig. 2). The lattice sites in the 2D and 3D systems in units of the lattice spacing  $a$  are located at the coordinates  $(x, y) = (\pm[n + 1/2], \pm[n + 1/2])$  and  $(x, y, z) = (\pm[n + 1/2], \pm[n + 1/2], \pm[n + 1/2])$ , respectively, where  $n = 0, 1, \dots, L/2 - 1$ . The linear extents of the systems with quadratic and quartic traps are  $L/a = 50$  in 2D and  $L/a = 14$  in 3D. With the trap curvatures and the range of the chemical potential offsets  $\mu_0/U$  that we have used, these system sizes ensure that the effective chemical potential takes large enough negative values at the boundaries of the systems for the particles to never reach the boundaries. The linear extents of the systems with closed boxes and the homogeneous systems with periodic boundary conditions have been reduced to  $L/a = 32$  and  $L/a = 28$  in 2D and  $L/a = 8$  in 3D to approximatively match the effective number of bosons trapped in the quadratic and quartic traps, i.e., the sizes of the regions with a nonvanishing local density.

### III. RESULTS

In this section we present the results obtained from simulations of the two- and three-dimensional Bose-

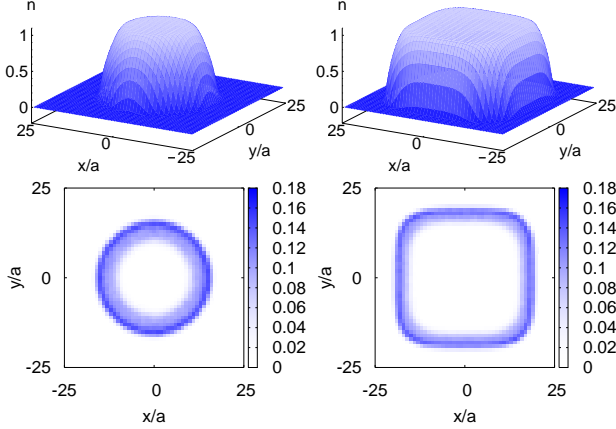


FIG. 3: (Color online) Spatial dependence of the local density  $n$  measured in the canonical ensemble (top), and of the local compressibility  $\kappa^{\text{local}} t$  measured in the grand-canonical ensemble (bottom) for 2D systems of size  $50 \times 50$  containing respectively 600 bosons in a quadratic trap with curvature  $a_2/U = 2 \cdot 10^{-3}$ , chemical potential offset  $\mu_0/U = 0.370$  and hopping parameter  $t/U = 0.04$  (left) and 1200 bosons in a quartic trap with curvature  $a_4/U = 3.5 \cdot 10^{-6}$ , chemical potential offset  $\mu_0/U = 0.362$  and the same hopping parameter  $t/U = 0.04$  (right). The special four-fold symmetry of the quartic trap is clearly reflected by the shape of the superfluid shell between the outer  $n = 0$  and the central  $n = 1$  Mott plateaus (right).

Hubbard model in quartic traps and compare results for quadratic traps with closed box configurations and homogeneous systems with periodic boundary conditions. Tables I and II give an overview of the simulation parameters in the canonical and grand-canonical ensemble, respectively.

First, we investigate quantum criticality at the *surface* which separates the superfluid and Mott-insulating states, which is shell-structured in systems with quadratic and quartic traps. Our results suggest that in regards to quantum criticality at the surface quadratic and quartic traps are equivalent: both systems show the same lack of quantum criticality. Next, we study quantum criticality to the *center* of the traps by restricting the measurements to small regions around the center. We drive these regions through the superfluid–Mott insulator transition and show that this *bulk* transition in the center of quartic traps has enhanced critical fluctuations in comparison to the center of quadratic traps.

#### A. Quantum criticality on the boundary between superfluid and Mott-insulating regions

We compare a system with a quadratic trap containing 600 bosons and a system with a quartic trap containing 1200 bosons. The hopping parameter is  $t/U = 0.04$  in both cases and the chemical potential offsets are

$\mu_0/U = 0.370$  in the quadratic case and  $\mu_0/U = 0.362$  in the quartic case. In both cases a Mott-insulating plateau with integer density  $\langle n_i \rangle = 1$  is present at the center of the trap, which is surrounded by a superfluid ring-like region, as depicted in Fig. 3, where the spatial dependence of the local density  $n$  and of the local compressibility  $\kappa^{\text{local}}$ , is shown. The left panels show the quadratic case and the right panels the quartic case. In both cases, the local compressibility takes its largest values close to the outer boundary of the superfluid shell. The shape of the superfluid shell clearly reflects the special four-fold rotational symmetry of the quartic trap, compared to the quadratic trap, which has a continuous rotational symmetry. Furthermore, the width of the superfluid shell is clearly smaller in the quartic trap than in the quadratic trap, which is due to the larger steepness of the former in the corresponding regions of the superfluid shell.

A better quantitative description of the systems in the two different traps is given by the radial dependence of the observables from the center towards the boundaries of the systems. In the quadratic case, due to the continuous rotational symmetry, the values at all lattice sites can be used to create such geometric profiles. In the quartic case, we are limited by the four-fold symmetry of the underlying potential and we thus use only points lying on the sections through the center and parallel to the boundaries of the systems. This limitation no longer applies to quartic traps when we plot local quantities as a function of the local effective chemical potential  $\mu^{\text{eff}}/U$ , since, as follows from the data collapse on single curves, cf. Fig. 5, a local potential approximation holds just as for quadratic traps [12], i.e., these quantities can be determined from the value of the local effective chemical potential.

The errors have been determined by means of a non-parametric bootstrap analysis [20] applied to each set of values corresponding to the same radial distance from the center or to the same effective chemical potential. If the error bars are not visible, they are smaller than the corresponding point sizes.

The radial dependence of the local density  $n$ , the local compressibility  $\kappa^{\text{local}}$ , the onsite compressibility  $\kappa^{\text{onsite}}$  and the variance  $\Delta$  for the same systems introduced above are given in Fig. 4. Noninteger local densities correspond to regions where the system is in the superfluid state, whereas integer local densities indicate regions in which the system is in the Mott-insulating state. The local compressibility profile consists of an asymmetric double-peak, which reflects the increase of the particle number fluctuations near the boundaries of the Mott-insulating regions. Both peaks are of the same height in the corresponding hard-core model due to particle-hole symmetry [12]. The onsite compressibility,  $\kappa^{\text{onsite}}$ , and the variance,  $\Delta$ , both peak inside the superfluid shell, but in contrast to the local compressibility,  $\kappa^{\text{local}}$ , they do not completely vanish inside the central Mott plateau. This is due to virtual hopping processes that are completely suppressed only by an infinite energy gap in the

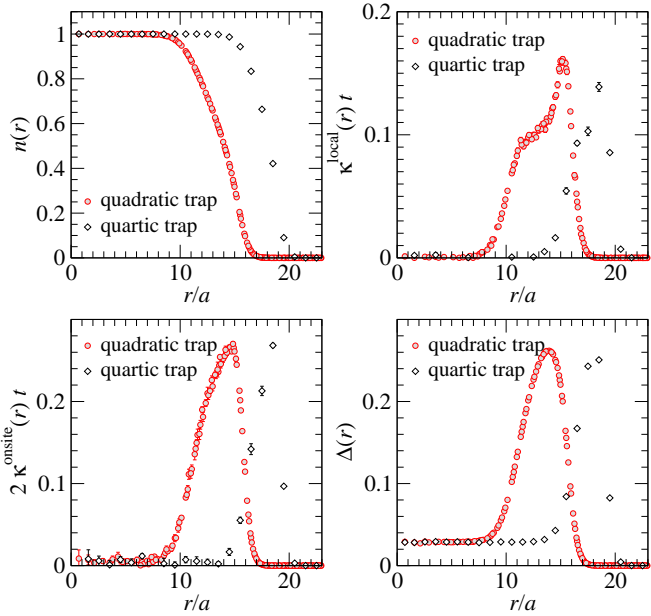


FIG. 4: (Color online) Radial dependence of the local density  $n$ , the local compressibility  $\kappa_{\text{local}}$ , the onsite compressibility  $\kappa_{\text{onsite}}$  and the variance  $\Delta$  for the same systems as in Fig. 3. All quantities are measured in the canonical ensemble, except for  $\kappa_{\text{local}}$  that can only be measured in the grand-canonical ensemble.

limit  $t/U \rightarrow 0$  [12]. As for the quadratic traps [12], we find for the quartic traps that  $\kappa_{\text{local}}$  is a better probe than  $\kappa_{\text{onsite}}$  and  $\Delta$  for the existence of superfluid and Mott-insulating regions. It can, therefore, serve as a genuine order parameter to characterize the superfluid–Mott insulator transition.

In Fig. 5 we show the local density  $n$  and the local compressibility  $\kappa_{\text{local}}$  as functions of the local effective chemical potential  $\mu^{\text{eff}}/U$ , which, as pointed out in Ref. 12, are not universal functions, but depend on both the geometries and the curvatures of the traps. The data for both quantities taken from the simulations with quadratic and quartic traps match almost perfectly. As a comparison, both curves are plotted for closed-box systems confined by completely flat and infinitely sharp traps as well as for homogeneous systems with periodic boundary conditions, all of size  $32 \times 32$ . This smaller size is comparable to the effective sizes of the systems with the quadratic and the quartic traps. Since in these uniform cases the effective chemical potential remains constant over the whole system, a whole set of simulations, each of which is performed with a different chemical potential, is needed in order to obtain these additional curves. In the local density curve, cusps appear at the points where the density approaches  $n = 0$  and  $n = 1$  and correspondingly both singularities in the local compressibility are more pronounced, indicating quantum criticality. As shown in Ref. 12, these cusps in  $n(\mu^{\text{eff}}/U)$  become smoother as the curvature is increased from zero (uniform case) to finite, positive values. This is due to the gradient in the con-

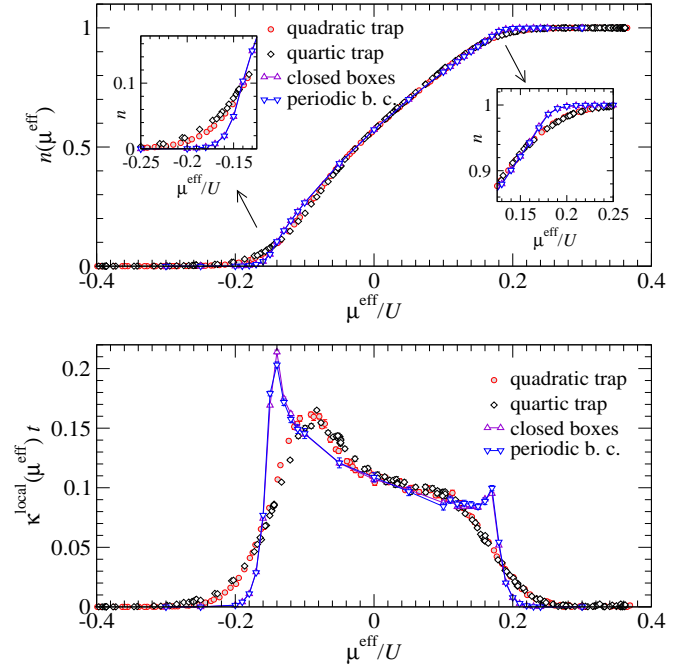


FIG. 5: (Color online) Local density  $n$  (top) and local compressibility  $\kappa_{\text{local}}$  (bottom), measured in the grand-canonical ensemble, vs the local effective chemical potential  $\mu^{\text{eff}}/U$ . The quadratic and quartic trap cases are the same as Fig. 3. We also show systems in closed boxes of size  $32 \times 32$  as well as homogeneous systems with periodic boundary conditions also of size  $32 \times 32$ . In all system, the hopping parameter is  $t/U = 0.04$ .

fining potential that becomes increasingly relevant and which destroys the quantum criticality. No quantum critical behavior is found for the transition at the surface separating the coexisting superfluid and Mott-insulating states in the quartic trap, in spite of its flatness in the center and the larger steepness of its walls.

## B. Bulk quantum criticality in the trap center

Instead of investigating the transition at the surface separating the coexisting superfluid and Mott-insulating states in the systems with quadratic and quartic traps, we now focus on the center of these traps and drive the local state through the superfluid–Mott insulator transition, which can be induced by either increasing the chemical potential offset  $\mu_0/U$  or by decreasing the ratio  $t/U$  between the hopping and the interaction parameter. The latter case, which is more likely to be reproduced experimentally, is shown in Fig. 7, where the local density  $n$  and the local compressibility  $\kappa_{\text{local}}$  are plotted against  $t/U$  at constant chemical potential  $\mu/U = 0.217$ . This scan is marked with a dashed line in Fig. 6 where the phase diagram of the homogeneous Bose-Hubbard model [3] is depicted schematically. At each point of the scan, both  $n$  and  $\kappa_{\text{local}}$  are measured at the twelve lattice sites that

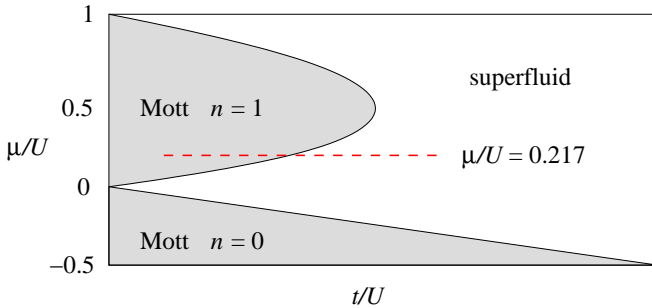


FIG. 6: (Color online) Phase diagram of the homogeneous Bose-Hubbard model [3]. It consists of a series of Mott-insulating lobes that are surrounded by a superfluid region. Each of the Mott lobes is characterized by an integer filling of single lattice sites. Here, only the  $n = 0$  and  $n = 1$  Mott lobes are shown. The constant- $(\mu/U = 0.217)$  scans presented in Figs. 7 and 8 are indicated by the dashed, horizontal line.

are closest to the center, i.e., at the four central lattice sites [19] and at their eight nearest neighbors (cross configuration). In 2D, with our chosen system sizes and trap curvatures, the difference of the effective chemical potential felt by bosons on the four central lattice sites and the one felt by bosons on their nearest neighbor lattice sites is negligible and thus the values measured at the nearest neighbor lattice sites can be included to enhance the statistics without falsifying the results. The curves originating from the system with the quartic trap almost match the curves originating from the uniform systems with closed boxes and periodic boundary conditions, whereas for the curves obtained from the system with the quadratic trap, the deviations are much stronger. The sharp cusp in the  $\kappa^{\text{local}}$  curve of the system with the quartic trap indicates the increase of critical fluctuations inside the trap and will diverge in the continuum limit. This special behavior demonstrates that locally at the center, the bulk transition from the superfluid to the Mott-insulating state exhibits stronger critical fluctuations in the quartic trap than in the quadratic trap.

Similarly as in 2D, we have performed the same constant- $(\mu/U = 0.217)$  scans through the critical point also for 3D systems, see Fig. 6. In contrast to the 2D case, the local density  $n$  and the local compressibility  $\kappa^{\text{local}}$  have been measured only at the eight central lattice sites [19]. Due to the smaller system sizes and the larger trap curvatures than in 2D, the twenty-four nearest neighbors lattice sites could not be considered since the effective chemical potentials at these nearest neighbors lattice sites and at the central lattice sites differ significantly from each other and thus correspond to two different scan lines in the phase diagram. As can be extracted from Fig. 8, the same yet less pronounced behavior in regards of bulk quantum criticality is observed, i.e., locally at the center of the traps, the transition from the local superfluid to the local Mott-insulating state is found to have slightly stronger critical fluctuations in the

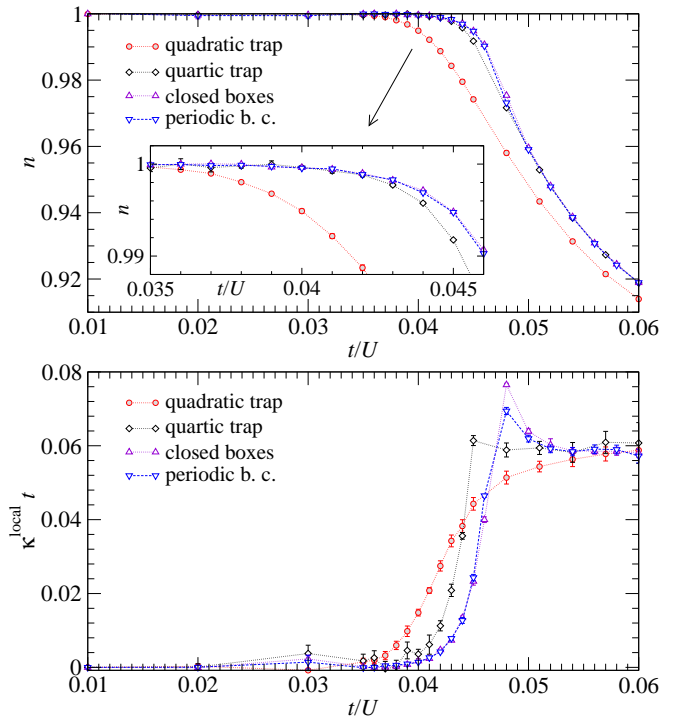


FIG. 7: (Color online) Constant- $(\mu/U = 0.217)$  scans through the critical point. The density  $n$  (top) and the local compressibility  $\kappa^{\text{local}}$  (bottom), in the grand-canonical ensemble, vs  $t/U$  for 2D systems of  $50 \times 50$  sites. The quadratic trap curvature is  $a_2/U = 2 \cdot 10^{-3}$  and the quartic trap curvature  $a_4/U = 3.5 \cdot 10^{-6}$ . Both quantities are measured at the center of the traps. For comparison, the same scans are plotted for a system in a closed-box and one with periodic boundary conditions of size  $28 \times 28$ .

quartic than in the quadratic trap. However, care must be taken while interpreting these results, due to the finite size effects that strongly affect the centers of these small 3D systems with their significantly reduced linear extents, compared to the 2D systems presented above.

#### IV. CONCLUSIONS

Ultracold bosonic atoms in optical lattices have been studied in quadratic and quartic traps. The physics of these confined systems is almost perfectly captured by the Bose-Hubbard model [1]. The specific traps can be taken into account by a site-dependent effective chemical potential in the Bose-Hubbard Hamiltonian. Our results in 2D clearly demonstrate that the quantum criticality of the transition at the surface layer separating the coexisting superfluid and Mott-insulating states is destroyed by the finite gradient of the trapping potential, even for traps with quartic profiles, which have steep walls and in whose centers the gradient almost vanishes. However, we have found that, if the measurements are restricted to the center of the traps and the local state is driven through the superfluid–Mott insulator transition, the then ob-

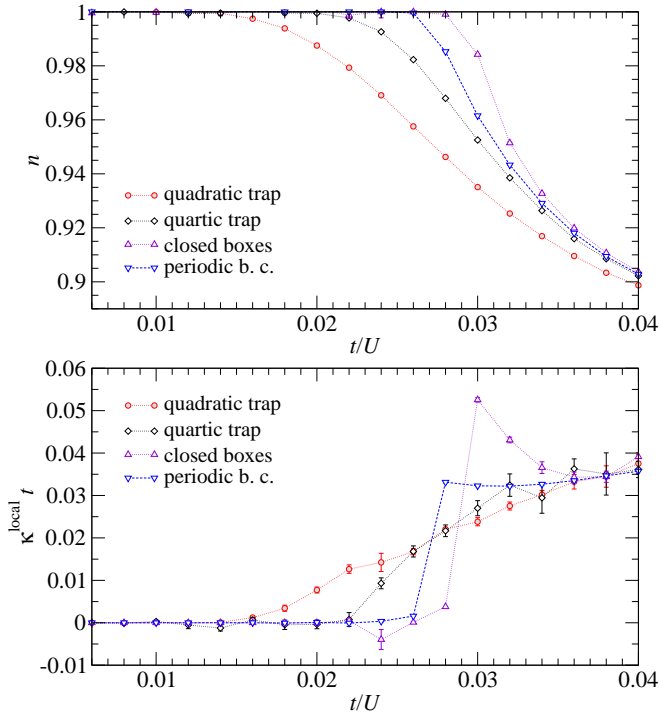


FIG. 8: (Color online) Constant- $(\mu/U = 0.217)$  scans through the critical point. The density  $n$  (top) and the local compressibility  $\kappa_{\text{local}}$  (bottom), in the grand-canonical ensemble, are plotted for 3D systems of  $14^3$  sites in a quadratic trap (curvature  $a_2/U = 0.03$ ) and in a quartic trap (curvature  $a_4/U = 7 \cdot 10^{-4}$ ). As in the 2D scans (Fig. 7),  $n$  and  $\kappa_{\text{local}}$  are measured at the center of the traps. For comparison, the same scans are plotted for closed-box systems and homogeneous systems with periodic boundary conditions of size  $8^3$ , which approximatively corresponds to the effective sizes of the systems with the quadratic and quartic traps.

served bulk transition has stronger critical fluctuations in quartic traps than in quadratic traps. To demonstrate

this, we use the local compressibility as a genuine, local order parameter to characterize the transition and drive the system center from the superfluid to the Mott-insulating state by decreasing the ratio  $t/U$  between the hopping and the interaction parameter at constant chemical potential  $\mu/U$ . The deviations of the curves obtained from the systems with quartic traps from the curves obtained from uniform systems with closed boxes and periodic boundary conditions are much less pronounced than the deviations of the curves obtained from the systems with quadratic traps. Even if there is no perfect match, we expect the quartic traps to constitute a remarkably better prerequisite for the experimental detection of true quantum criticality.

Our simulations of moderately-sized 3D systems lead to the same conclusions as in 2D, but, due to strong finite size effects present in these systems, an analysis with yet larger systems is desirable.

Finally, it is worth mentioning that quartic traps represent an ideal for traps that are experimentally realized by superimposing blue- to red-detuned laser beams with Gaussian intensity profiles. The flatness achievable in the trap center depends on the ability to suppress the quadratic terms in the series expansion of the resulting confining potential. Since this might turn out to be a rather difficult task, it could be interesting to investigate what influence small fluctuations in the otherwise flat trap centers have on the local bulk quantum criticality.

## Acknowledgments

The simulations have been performed on the Hreibdar and Gonzales clusters at ETH Zürich using the worm algorithm [16] and the SSE algorithm with directed loops [17] of the ALPS [15] project. We thank T. Esslinger, M. Köhl and S. Trebst for helpful discussions.

- 
- [1] D. Jaksch, C. Bruder, J. I. Cirac, C. W. Gardiner, and P. Zoller, *Cold Bosonic Atoms in Optical Lattices*, Phys. Rev. Lett. **81**, 3108 (1998).
- [2] M. Greiner, O. Mandel, T. Esslinger, T. W. Hänsch, and I. Bloch, *Quantum phase transition from a superfluid to a Mott insulator in a gas of ultracold atoms*, Nature **415**, 39 (2002).
- [3] M. P. A. Fisher, P. B. Weichman, G. Grinstein, and D. S. Fisher, *Boson localization and the superfluid-insulator transition*, Phys. Rev. B **40**, 546 (1989).
- [4] P. Niyaz, R. T. Scalettar, C. Y. Fong, and G. G. Batrouni, *Phase transitions in an interacting boson model with near-neighbor repulsion*, Phys. Rev. B **50**, 362 (1994).
- [5] W. Zwerger, *Mott-Hubbard transition of cold atoms in optical lattices*, J. Opt. B **5**, S9 (2003).
- [6] G. G. Batrouni, R. T. Scalettar, and G. T. Zimanyi, *Quantum critical phenomena in one-dimensional Bose systems*, Phys. Rev. Lett. **65**, 1765 (1990).
- [7] G. G. Batrouni and R. T. Scalettar, *World line simulations of the bosonic Hubbard model in the ground state*, Comput. Phys. Commun. **97**, 63 (1996).
- [8] J. K. Freericks and H. Monien, *Strong-coupling expansions for the pure and disordered Bose-Hubbard model*, Phys. Rev. B **53**, 2691 (1996).
- [9] V. A. Kashurnikov, N. V. Prokof'ev, and B. V. Svistunov, *Revealing the superfluid-Mott-insulator transition in an optical lattice*, Phys. Rev. A **66**, 031601 (2002).
- [10] G. Schmid, S. Todo, M. Troyer, and A. Dorneich, *Finite-Temperature Phase Diagram of Hard-Core Bosons in Two Dimensions*, Phys. Rev. Lett. **88**, 167208 (2002).
- [11] G. G. Batrouni, V. Rousseau, R. T. Scalettar, M. Rigol, A. Muramatsu, P. J. Denteneer, and M. Troyer, *Mott Domains of Bosons Confined on Optical Lattices*, Phys. Rev. Lett. **89**, 117203 (2002).
- [12] S. Wessel, F. Alet, M. Troyer, and G. G. Batrouni, *Quan-*

- tum Monte Carlo simulations of confined bosonic atoms in optical lattices, Phys. Rev. A **70**, 053615 (2004).
- [13] S. Wessel, F. Alet, S. Trebst, D. Leumann, M. Troyer, and G. G. Batrouni, *Bosons in optical lattices - from the Mott transition to the Tonks-Girardeau gas*, J. Phys. Soc. Jpn. Suppl. **74**, 10 (2005).
- [14] E. L. Pollock and D. M. Ceperley, *Path-integral computation of superfluid densities*, Phys. Rev. B **36**, 8343 (1987).
- [15] F. Alet, P. Dayal, A. Grzesik, M. Honecker, A. Laeuchli, S. R. Manmana, I. P. McCulloch, F. Michel, R. M. Noack, G. Schmid, et al., *The ALPS project: open source software for strongly correlated systems*, J. Phys. Soc. Jap. Suppl. **74**, 30 (2005).
- [16] N. V. Prokof'ev, B. V. Svistunov, and I. S. Tupitsyn, *“Worm” algorithm in quantum Monte Carlo simulations*, Phys. Lett. A **238**, 253 (1998).
- [17] F. Alet, S. Wessel, and M. Troyer, *Generalized directed loop method for quantum Monte Carlo simulations*, Phys. Rev. E **71**, 036706 (2005).
- [18] For example, in the constant- $\mu/U$  scan presented in Fig. 6, the filling of the uniform system along the part of the scan that lies in first Mott lobe is necessarily commensurate, whereas the filling along the part of the scan that lies in the surrounding superfluid region is in general incommensurate. Furthermore, for the simulations at constant  $\mu/U$  of the systems with quadratic and quartic traps, the particle number slightly depends on  $t/U$ .
- [19] Note that, since all our 2D and 3D systems have an even number of lattice sites, there is no lattice site at the center of the system, at which the observables can be measured for the constant- $(\mu/U)$  scans. The observables are thus measured at the closest lattice sites that surround the center. For each system with quadratic or quartic traps, the values of the chemical potential offsets  $\mu_0/U$  have been chosen in such a way that the effective chemical potential  $\mu_{\text{center}}^{\text{eff}}/U$  at these central lattice sites coincides with the chemical potential  $\mu/U = 0.217$  chosen for the uniform systems.
- [20] B. Efron, *Bootstrap methods: another look at the Jackknife*, Ann. Statist. **7**, 1 (1979).